Contribution of C−H···π interactions to polymorphic transitions of a molecular crystal with disordered fragments

Takuya Taniguchi,[*1] *Daisuke Takagi,*[2] *Toru Asahi*[2,3,4]

[1] Center for Data Science, Waseda University, 1-6-1 Nishiwaseda, Shinjuku-ku, Tokyo 169-0051, Japan

[2] Department of Life Science and Medical Bioscience, School of Advanced Science and Engineering, Waseda University, 3-4-1 Okubo, Shinjuku-ku, Tokyo 169-8555, Japan

[3] Department of Life Science and Medical Bioscience, Graduate School of Advanced Science and Engineering, Waseda University, 3-4-1 Okubo, Shinjuku-ku, Tokyo 169-8555, Japan

[4] Research Organization for Nano & Life Innovation, Waseda University, 513 Wasedatsurumaki-cho, Shinjuku-ku, Tokyo 162-0041, Japan

* To whom correspondence should be addressed.

E-mail: takuya.taniguchi@aoni.waseda.jp

Abstract

Polymorphic transition is important for the functionality of crystalline materials. However, the underlying mechanism remains unclear, especially when the crystal structure contains disordered fragments. We report that C−H···π interactions play an important role in polymorphic transitions in a molecular crystal with disordered fragments. The crystal has three phases, namely the α (< -80°C), β (-80–40°C), and γ (< 40°C) phases, which are reversible through single-crystal-to-single-crystal transformation in association with temperature change. Disorder of bulky *tert*-butyl substituents appears at high-temperature in the β and γ phases. Intermolecular interaction analysis based on Hirshfeld surfaces and related fingerprint plots revealed that the proportion of π···π interactions decreased, while that of C−H···π interactions increased, at the transition from α to β phase. The proportion of C−H···π interactions also increased at the transition from β to γ phase, but continuously decreased in the β phase due to elevated temperature. Intermolecular interaction energies clarified the contribution of C−H···π interactions to the stability of high-temperature crystal β and γ phases via polymorphic transitions. Our results potentially lead to design molecular crystals with polymorphic transitions.

Introduction

Polymorphic transitions in molecular crystals refer to the change in crystal structure induced by external stimuli, and are fundamental for expressing material functionalities. Polymorphic transition has many applications, including organic electronics, magnetics, actuators, and pharmaceuticals [1–5]. For example, ferroelectric molecular crystals manifest their ferroic properties below the transition temperature [1,2]. In addition, dozens of molecular crystals exhibit actuation behaviors, such as elongation/contraction, bending, and jump, at the transition temperature [6–13]. Thus, polymorphic transitions are of importance both to increase our fundamental understanding of transitions and for potential industrial applications.

Realizing polymorphic transitions of molecular crystals is important for optimal functionality and effective use of resources. While previous reports have aimed at prediction and simulation of the conditions required for polymorphic transitions in molecular crystals [14–18], they are, in general, still difficult to predict. Thus, our understanding of the underlying mechanism remains unclear. The main challenge is that high computation accuracy is required to identify the small difference of crystal structures due to the degree of freedom of molecular conformations and alignments. In addition, when the crystal structure is disordered, as reported for some polymorphic transitions [11,19,20], the

theoretical simulations become more complicated. Therefore, the inductive approach, i.e., obtaining knowledge from data [21], can be applied to increase our understanding, and design polymorphic transitions, of molecular crystals.

Recently, we reported on the polymorphic transitions of a molecular crystal of a salicylideneamine compound (referred to as enol-(*S*)-**1**, Fig. 1a) [22]. The enol-(*S*)-**1** crystal has three crystal phases, namely α (< -80°C), β (-80–40°C), and γ (< 40°C) phases, and *tert*-butyl substituents are disordered at β and γ phases (Fig. 1b,c). Polymorphic transitions occur at around −80 and 40°C through single-crystal-to-single-crystal transformation, with small transition enthalpies of 1.2 and 0.2 kJ/mol, respectively. The transition enthalpies are relatively small even when compared to those of other typical polymorphic transitions [6–12,19,20], and thus the mechanism of this thermal polymorphic transitions is to be investigated.

Here, we report that the C−H···π interactions contribute to the stability of high-temperature crystal phases of enol-(*S*)-**1**, as revealed by intermolecular interaction analyses. The Hirshfeld surface analyses and related fingerprint plots, which can be used to map intermolecular interactions [23–25], revealed that the proportion of π···π interactions decreased, while that of C−H···π interactions increased, after the transition from the α to β phase. The proportion of C−H···π interaction decreased

in the β phase due to the temperature rise, but slightly increased after the transition from the β to γ phase. Intermolecular interaction energies in these crystal phases were also calculated based on density functional theory (DFT) and dispersion correlation, and indicated that the energies of C−H···π interactions stabilized after the transition both the α to β phase, and from the β to γ phase. These results support the contribution of C−H···π interactions to the stability of high-temperature crystal phases. This work will aid the design of polymorphic transitions for crystal functionalities.

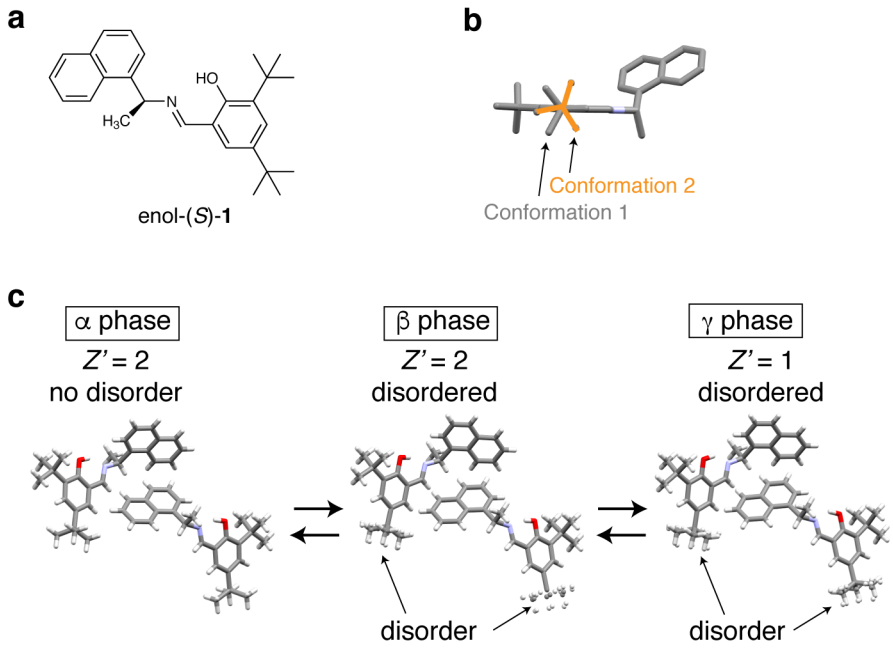

Figure 1. Polymorphic transitions of the enol-(*S*)-**1** crystal. (a) Molecular structure of enol-(*S*)-**1**. (b) Disordered conformations of the *tert*-butyl substituent. (c) Crystal phases related by polymorphic transitions.

Results and Discussion

Hirshfeld surface analysis. Since the crystal structures of enol-(*S*)-**1**, obtained from Cambridge Crystallographic Data Centre, are disordered at *tert*-butyl substituents in the β and γ phases, the .cif files of the disordered structures were edited to yield ordered structures for the Hirshfeld surface and intermolecular interaction energy analyses (see Methods section and Supplementary Figure 1). This editing procedure is accepted for the analysis of disordered crystals, as reported previously [26]. The Hirshfeld surfaces and related fingerprint plots can be used to analyze the interaction motifs and contributions [23–25]. Figure 2a shows the Hirshfeld surface of an enol-(*S*)-**1** molecule and surrounding molecules, viewed from (100) face in the α phase (−100°C). To identify interaction pairs, the center molecule and surrounding molecules are represented as coordinates according to their relative positions (Fig. 2b). The first numbers (0–6) represent the relative positions projected on (100) plane, while the second notations +, 0, and – represent the relative heights of the projected molecules along the *a*-axis. Three molecules are stacked along the *a*-axis at positions 0, 1, and 4, where the second notation becomes +, 0, or –. At positions 2, 3, 5, and 6, two molecules stack and thus + or – is used as the relative height. As such, the center molecule is labeled as (0,0), and molecule pairs can be represented as (0,0)–(0,+), (0,0)–(1,0), and so on. This index rule should be superior to symmetry

codes when crystal structures belong to different space groups; in this case, $P1$ (in the α and β phases) and $P2_1$ (in the γ phase). Another notice is that indexed pairs are unifiedly represented even when Z'=2. This is because the same interaction motifs can be identified even when molecules around each independent molecule are indexed differently (Supplementary Figure 2). According to this index rule, interaction motifs were characterized using the structure in the α phase (Fig. 2c–e and Table 1). C−H···O interactions were formed along the *b* axis at the (0,0)–(1,0) and (0,0)–(4,0) pairs, which are related by the translational symmetry operation along the *b*-axis (Fig. 2c). π···π interactions occurred along the *a* axis at the (0,0)–(0,+) and (0,0)–(0,−) pairs, which are also related by the translational operation along the *a*-axis (Fig. 2d). C−H···π interactions occurred at the (0,0)–(2,+), (0,0)–(2,−), (0,0)–(3,+), and (0,0)–(3,−) pairs, where the naphthyl ring of (0,0) is almost perpendicular to the surrounding naphthyl rings of (2,+), (2,−), (3,+), and (3,−) (Fig. 2e). These three types of interactions contributed mainly to the crystal packing, not only in the α phase, but also in the β and γ phases, since molecular packing is largely similar among the three crystal phases. Interactions at the other pairs should be mediated by weak van der Waals interactions.

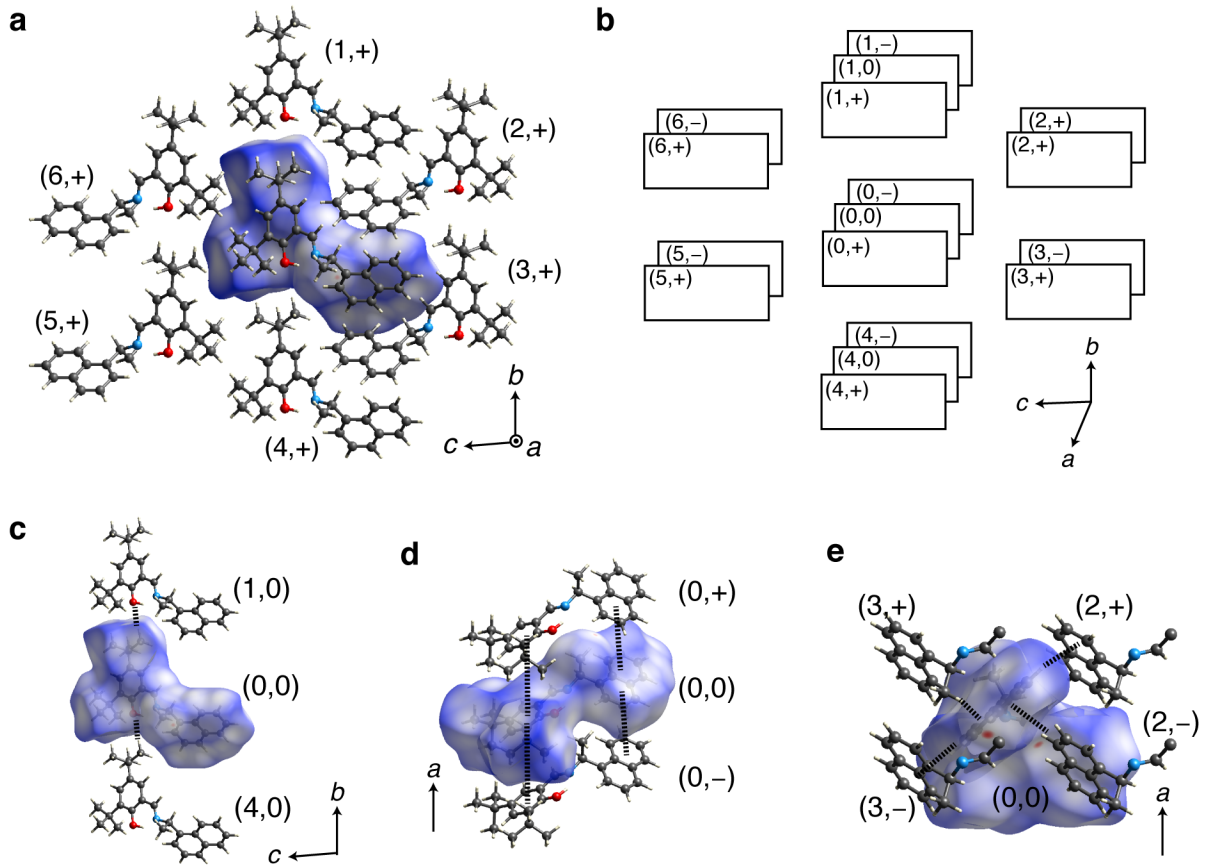

Figure 2. Interaction motifs and index rule. (a) Packing geometry around the Hirshfeld surface of the center molecule and surrounding molecules, viewed along the *a*-axis. (b) Index rule according to the relative positions. (c–e) Specific interaction motifs of (c) the C−H···O interaction along the *b*-axis, (d) π···π interaction along the *a*-axis, and (e) C−H···π interaction between naphthyl rings.

Table. 1 Identification of molecule pairs and the main interaction motifs

Molecular pairs with (0,0)	Main interaction motif
(0,+) and (0,–)	π···π interaction
(1,0) and (4,0)	C−H···O interaction

(2,+), (2,–), (3,+), and (3,–)	C−H···π interaction
(1,+), (1,–), (4,+), (4,–), (5,+), (5,–), (6,+), and (6,–)	van der Waals interaction

We next analyzed two-dimensional (2D) Hirshfeld fingerprint plots to compare interaction motifs among crystal phases. The plot shows the distribution of d_i and d_e, where d_i and d_e are the distances from a point on the Hirshfeld surface to the nearest nucleus inside and outside the surface, respectively. The major contact type is H···H contact, which should reflect van der Waals interactions, followed by C···H and H···C contacts, which should reflect C−H···π interactions (Fig. 3a,b). In both cases, wing-like distributions, which appeared in the α phase, disappeared in the β phase, with no distinct change between the β and γ phases. The distribution of O···H and H···O contacts, which should reflect C−H···O interactions, showed arrow-like shapes, which became blurry in high-temperature phases (Fig. 3c). The distribution of C···C contact, which reflects the strength of the π···π interaction [27], is a rather far distance, and changed distinctly between the α and β phases (Fig. 3d).

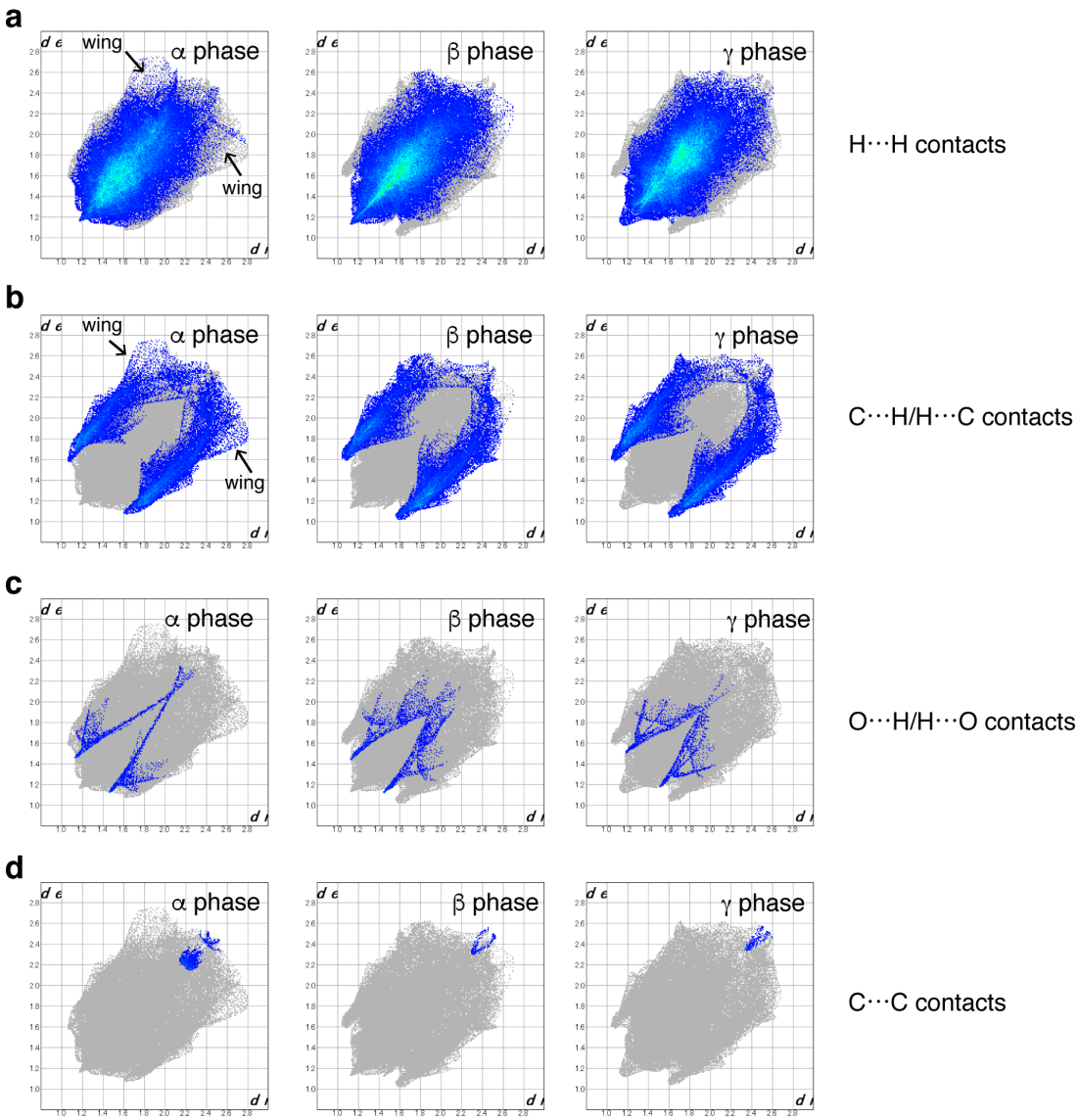

Figure 3. Comparison of 2D fingerprint plots between the α (–100°C), β (–50°C), and γ (60°C) phases. Mapping of (a) H···H, (b) C···H and H···C, (c) O···H and H···O, and (d) C···C contacts, respectively.

The temperature dependence behaviors of the interaction motifs in the α, β, and γ phases were evaluated in terms of the percentage contributions of each contact type. The major contact type was H···H in the α phase (–90°C) and β phase (–80°C), at 74.3% and 73.0%, respectively; its contribution continuously increased at β and γ phases with the temperature increase (Fig. 4a). By contrast, the percentage contribution of C···H/H···C contacts increased at the transition from the α to β phase, continuously decreased during the β phase depending on the temperature rise, and increased very slightly (from 23.2 to 23.3%) at the transition to the γ phase (Fig. 4b). This suggests that C−H···π interactions strengthened at the transition from the α to β phase, and from the β to γ phase. For O···H/H···O contacts, the percentage contribution did not change at the transition from the α to β phase, and continuously decreased depending on the temperature rise, supporting a weakening of C−H···O interactions (Fig. 4c). The percentage contribution of the C···C contact type, which reflects π···π interactions, decreased from 1.0% to 0.2% at the transition from the α to β phase, and was maintained during the β and γ phases (Fig. 4d). This result for C···C contact is consistent with the change in distribution seen in the 2D fingerprint plots, as shown in Fig. 3d. The temperature dependence of the percentage contributions of these contacts suggests that the C−H···π interaction is

more influential than the other interaction motifs with respect to the stability of high-temperature crystal phases.

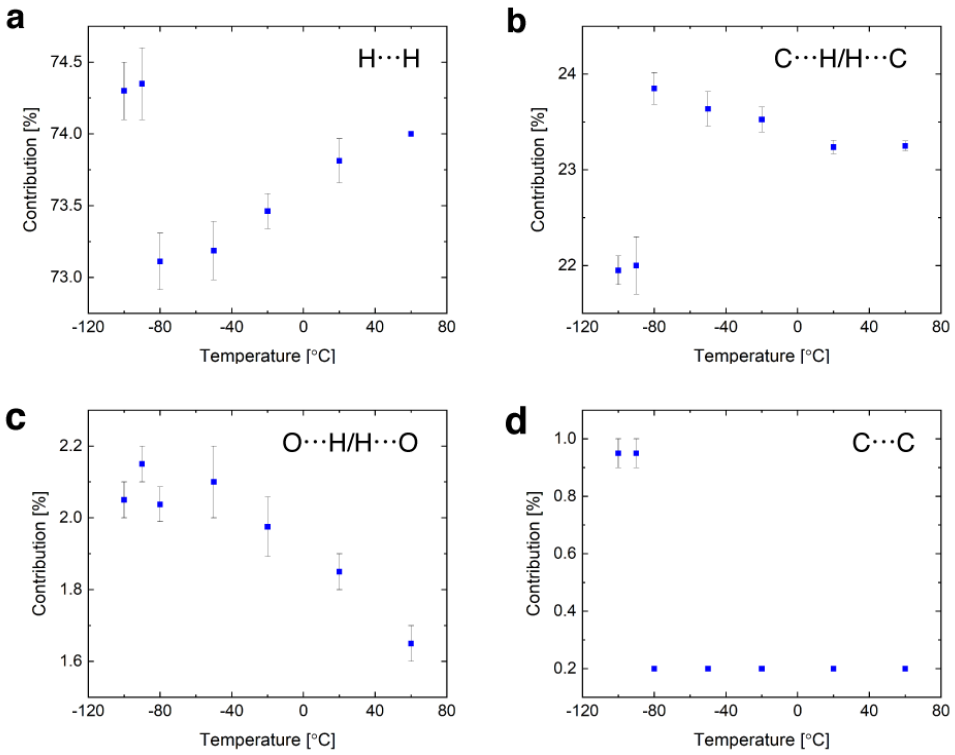

Figure 4. Temperature dependence of the percentage contributions of the interaction motifs. Each plot is the average value of the disordered structure at a given temperature. Error bars represent standard deviation based on the calculated results.

Intermolecular interaction energies. To explore the effect of interaction motifs on crystal stability, intermolecular interaction energies were calculated based on DFT and dispersion correlation (B3LYP-D2/6-31G(d,p); see Methods section for more details). The energy calculations for all pairs

were performed between the center molecule of (0,0) and surrounding molecules, as shown in Fig. 2. The calculations of the interaction energies of all pairs afforded 12 unique intermolecular interaction energies (Supplementary Figure 3). Among them, the six largest interaction energies were extracted for further discussion on crystal stability (Fig. 5). The largest interaction energy is that of the (0,0)–(0,+) and (0,0)–(0,–) pairs, between which π···π interactions are formed (Fig. 5a). The interaction energy was –42 kJ/mol in the α phase, which changed markedly at the transition to the β phase, and then continuously increased (i.e., became less stable) due to the temperature rise. The interaction energy of pairs (0,0)–(1,0) and (0,0)–(4,0), which reflect the C−H···O interaction motif, also tended to increase depending on the temperature increase (Fig. 5b).

In contrast to the π···π and C−H···O interactions, C−H···π interactions occurred for four different pairs: (0,0)–(2,+), (0,0)–(2,–), (0,0)–(3,+), and (0,0)–(3,–). The interaction energy of the (0,0)–(2,+) pair decreased (i.e., became more stable) at the transition from the α to β phase (Fig. 5c). While the interaction at the β phase became less stable depending on the temperature rise, the interaction stabilized slightly at the transition to the γ phase (Fig. 5c). For the (0,0)–(2,–) and (0,0)–(3,+) pairs, the interaction energies also decreased (i.e., became more stable) at the transition from the α to β phase, and continuously increased with no distinct change at the transition from the β to γ

phase (Fig. 5d,e). The interaction energy of the (0,0)–(3,−) pair increased at the transition from the α to β phase, and decreased (i.e., became more stable) at the transition from the β to γ phase (Fig. 5f). These results for the C−H···π interactions indicated that three interaction pairs stabilized at the transition from the α to β phase, and that two interaction pairs stabilized at the transition from the β to γ phase despite the temperature increase. This temperature dependence behavior of the C−H···π interaction motif is different from the π···π and C−H···O interactions, suggesting that C−H···π interactions contribute to stability by forming polymorphs at higher temperatures.

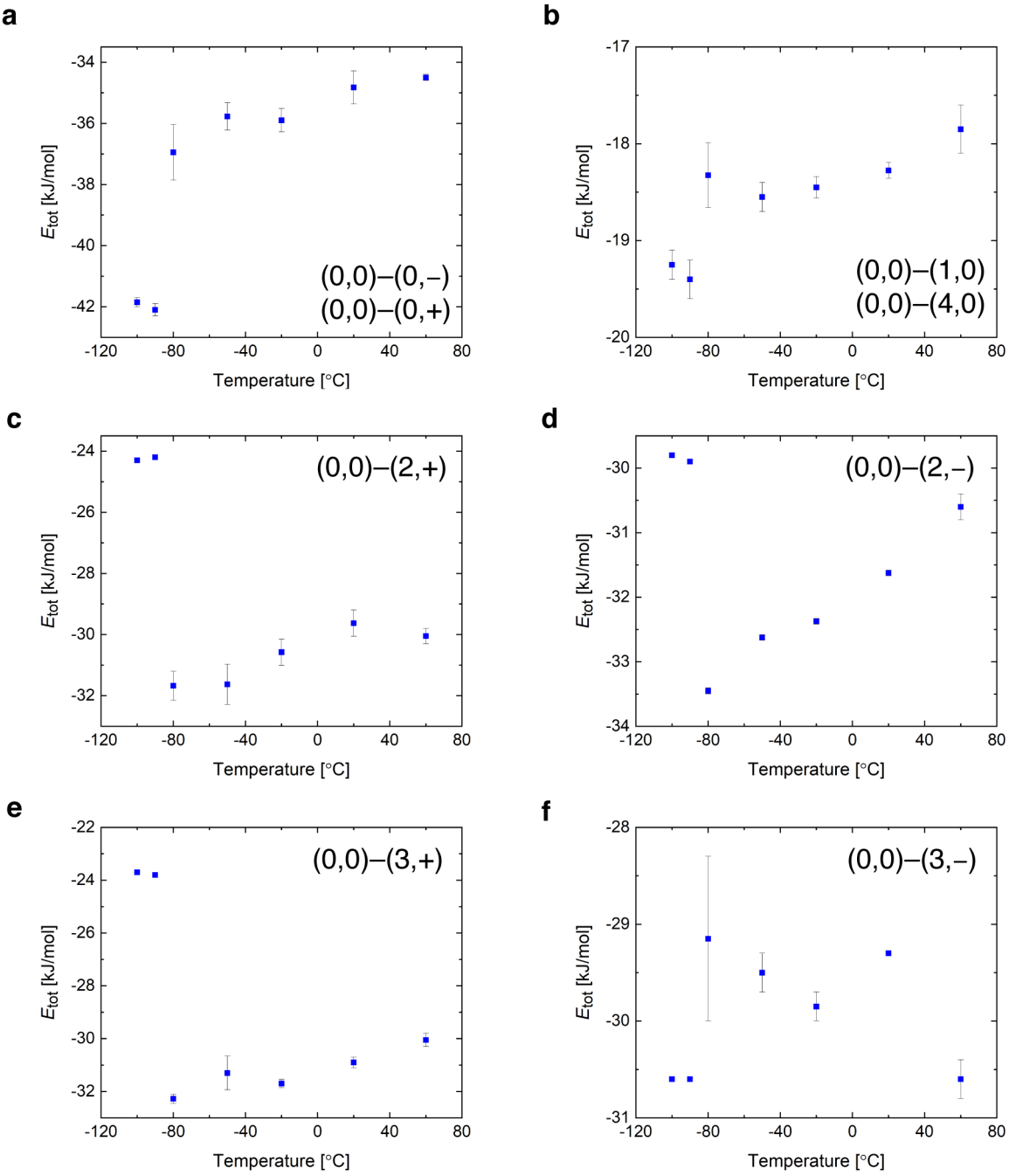

Figure 5. Temperature dependence of intermolecular interaction energies. Panels a–f show the six largest interaction energies among the calculated energies. In each panel, the interaction pair comprises the center molecule and a molecule in the position as shown in the graph. Plots show the

average value of all calculated results at a given temperature. Error bars represent standard deviation based on the calculated results.

Conclusions

Intermolecular interactions of the crystal structures of enol-(*S*)-**1**, which contain disordered fragments of the *tert*-butyl group, were investigated by Hirshfeld surface analyses, related 2D fingerprint plots, and analysis of intermolecular interaction energies. The Hirshfeld surfaces and fingerprint plots showed that the enol-(*S*)-**1** crystal consisted of three interaction motifs, namely, π···π, C−H···O, and C−H···π interactions (at the α, β, and γ phases). The percent contributions of C···C and O···H/H···O contacts, which reflect overall π···π and C−H···O interactions, decreased or did not change at the polymorphic transition from the α to β phase or β to γ phase. By contrast, the percentage contribution of C···H/H···C contacts, which reflects the overall C−H···π interaction, increased at these polymorphic transitions despite continuous decreases during the β phase with increasing temperature. The intermolecular interaction energies revealed that three of four energies, assigned to C−H···π interactions, stabilized at the transition from the α to β phase, and that two also stabilized at the transition from the β to γ phase. This unique behavior of the C−H···π interaction, compared to the

π···π and C−H···O interactions, supported the contribution of C−H···π interactions to the stability of high-temperature phases at polymorphic transitions. Our results provide a basis for performing intermolecular interaction analysis underlying polymorphic transitions and will aid the design of molecular crystals with polymorphic transitions.

Methods

Data manipulation

The crystallographic information files (CIF) of enol-(*S*)-**1** crystal at various temperatures were downloaded from the Cambridge Crystallographic Data Centre (CCDC) using the reference numbers 1879558–1879564. Since the crystal structures at β and γ phases contain disordered fragments of *tert*-butyl substituent, the .cif files of the disordered structures were edited (i.e., separated) to afford ordered structures. For example, the crystal structure at the γ phase has *Z*' = 1 with disorder between two conformations of the *tert*-butyl substituent; separation affords two .cif files. One file contains only major, and the other only minor, conformations, where the crystal structures are assumed to be ordered. For the β phase, separation affords four .cif files from each raw .cif file due to *Z*' = 2. See Supplementary Figure 1 for this scheme.

Computation of intermolecular interactions

The Hirshfeld surfaces were calculated based on molecular weight function using *CrystalExplorer17.5* [28–30]. The Hirshfeld surface surrounding a molecule can be obtained and visualized as a three-dimensional configuration, as described in previous reports [23–25]. The visualization, colored according to the d_{norm} property, represents close interactions between the internal and external molecules. By selecting atoms inside and outside the surface, the corresponding atom–atom contacts were colored. The 2D fingerprint plots of the Hirshfeld surface were represented by reciprocal coordinates with vertical axis d_e (distance from the surface to the closest nucleus outside the surface) and horizontal axis d_i (distance from the surface to the closest nucleus inside the surface. d_{norm} is the sum of d_i and d_e normalized by the van der Waals radius.

To calculate intermolecular interaction energies, all molecules having an atom within the van der Waals radius of 3.8–4.1 Å around a selected molecule were considered to afford surrounding 16 molecules. The intermolecular interaction energies are composed of four components, namely, electrostatic (E_{ele}), polarization (E_{pol}), dispersion (E_{dis}), and exchange-repulsion (E_{rep}) energies. The dispersion energy is Grimme's D2 dispersion correlation [31], and the intermolecular interaction

energies were calculated based on B3LYP-D2/6-31G(d,p) using *CrystalExplorer* 17.5. The total energy (E_{tot}) was calculated by summing these four energies, with scale factor coefficients of 1.057, 0.740, 0.871, and 0.618, respectively [29]. When the crystal structure has $Z' > 1$, calculations are performed independently for each independent molecule. The intermolecular interaction energy calculations were performed on a general desktop PC and each calculation took about 20 hours.

References

[1] Fu, D. W.; Cai, H. L.; Liu, Y.; Ye, Q.; Zhang, W.; Zhang, Y.; Chen, X. Y.; Giovannetti, G.; Capone, M.; Li, J.; Xiong, R. G. Diisopropylammonium bromide is a high-temperature molecular ferroelectric crystal. *Science* **2013**, *339*, 425–428.

[2] Cui, H.; Wang, Z.; Takahashi, K.; Okano, Y.; Kobayashi, H.; Kobayashi, A. Ferroelectric porous molecular crystal, $[Mn_3(HCOO)_6](C_2H_5OH)$, exhibiting ferrimagnetic transition. *J. Am. Chem. Soc.* **2006**, *128*, 15074–15075.

[3] Sato, O. Dynamic molecular crystals with switchable physical properties. *Nat. Chem.* **2016**, *8*, 644–656.

[4] Naumov, P.; Chizhik, S.; Panda, M. K.; Nath, N. K.; Boldyreva, E. Mechanically responsive molecular crystals. *Chem. Rev.* **2015**, *115*, 12440–12490.

[5] Kelmann, R. G.; Kuminek, G.; Teixeira, H. F.; Koester, L. S. Preliminary study on the development of nanoemulsions for carbamazepine intravenous delivery: An investigation of drug polymorphic transition. *Drug Dev. Ind. Pharm.* **2008**, *34*, 53–58.

[6] Liu, G.; Liu, J.; Liu, Y.; Tao, X. Oriented single-crystal-to-single-crystal phase transition with dramatic changes in the dimensions of crystals. *J. Am. Chem. Soc.* **2014**, *136*, 590–593.

[7] Shima, T.; Muraoka, T.; Hoshino, N.; Akutagawa, T.; Kobayashi, Y.; Kinbara, K. Thermally driven polymorphic transition prompting a naked-eye-detectable bending and straightening motion of single crystals. *Angew. Chem. Int. Ed.* **2014**, *53*, 7173–7178.

[8] Sahoo, S. C.; Sinha, S. B.; Kiran, M. S. R. N.; Ramamurty, U.; Dericioglu, A. F.; Reddy, C. M.; Naumov, P. Kinematic and mechanical profile of the self-actuation of thermosalient crystal twins of 1,2,4,5-tetrabromobenzene: A molecular crystalline analogue of a bimetallic strip. *J. Am. Chem. Soc.* **2013**, *135*, 13843–13850.

[9] Panda, M. K.; Runčevski, T.; Sahoo, S. C.; Belik, A. A.; Nath, N. K.; Dinnebier, R. E.; Naumov, P. Colossal positive and negative thermal expansion and thermosalient effect in a pentamorphic organometallic martensite. *Nat. Commun.* **2014**, *5*, 1–8.

[10] Dharmarwardana, M.; Welch, R. P.; Kwon, S.; Nguyen, V. K.; McCandless, G. T.; Omary, M. A.; Gassensmith, J. J. Thermo-mechanically responsive crystalline organic cantilever. *Chem. Commun.* **2017**, *53*, 9890–9893.

[11] Taniguchi, T.; Sugiyama, H.; Uekusa, H.; Shiro, M.; Asahi, T.; Koshima, H. Walking and rolling of crystals induced thermally by phase transition. *Nat. Commun.* **2018**, *9*, 1–8.

[12] Hagiwara, Y.; Taniguchi, T.; Asahi, T.; Koshima, H. Crystal actuator based on a thermal phase transition and photothermal effect. *J. Mater. Chem. C* **2020**, *8*, 4876–4884.

[13] Koshima, H.; Taniguchi, T.; Asahi, T. Mechanically Responsive Crystals by Light and Heat. Chapter 3 in *Mechanically Responsive Materials for Soft Robotics*, H. Koshima, Ed., **2020**, Wiley-VCH Verlag GmbH & Co. KGaA.

[14] Červinka, C.; Beran, G. J. *Ab initio* prediction of the polymorph phase diagram for crystalline methanol. *Chem. Sci.* **2018**, *9*, 4622–4629.

[15] Dybeck, E. C.; Abraham, N. S.; Schieber, N. P.; Shirts, M. R. Capturing entropic contributions to temperature-mediated polymorphic transformations through molecular modeling. *Cryst. Growth Des.* **2017**, *17*, 1775–1787.

[16] van den Ende, J. A.; Ensing, B.; Cuppen, H. M. Energy barriers and mechanisms in solid–solid polymorphic transitions exhibiting cooperative motion. *CrystEngComm* **2016**, *18*, 4420–4430.

[17] Anwar, J.; Zahn, D. Polymorphic phase transitions: Macroscopic theory and molecular simulation. *Adv. Drug Delivery Rev.* **2017**, *117*, 47–70.

[18] Piaggi, P. M.; Parrinello, M. Predicting polymorphism in molecular crystals using orientational entropy. *Proc. Nat. Acad. Sci.* **2018**, *115*, 10251–10256.

[19] Minami, T.; Sato, H.; Matsumoto, S. Macroscopic crystalline deformation in an organic dye during reversible phase transition caused by alkyl disorder. *CrystEngComm* **2018**, *20*, 2644–2647.

[20] Takanabe, A.; Katsufuji, T.; Johmoto, K.; Uekusa, H.; Shiro, M.; Koshima, H.; Asahi, T. Reversible single-crystal-to-single-crystal phase transition of chiral salicylidenephenylethylamine. *Crystals* **2017**, *7*, 7.

[21] Vologzhanina, A. V. Intermolecular interactions in functional crystalline materials: From data to knowledge. *Crystals* **2019**, *9*, 478.

[22] Taniguchi, T.; Sato, H.; Hagiwara, Y.; Asahi, T.; Koshima, H. Photo-triggered phase transition of a crystal. *Commun. Chem.* **2019**, *2*, 1–10.

[23] McKinnon, J. J.; Spackman, M. A.; Mitchell, A. S. Novel tools for visualizing and exploring intermolecular interactions in molecular crystals. *Acta Crystallogr. Sect. B: Struct. Sci.* **2004**, *60*, 627–668.

[24] Spackman, M. A.; McKinnon, J. J. Fingerprinting intermolecular interactions in molecular crystals. *CrystEngComm* **2002**, *4*, 378–392.

[25] Spackman, M. A.; Jayatilaka, D. Hirshfeld surface analysis. *CrystEngComm* **2009**, *11*, 19–32.

[26] Munshi, P.; Skelton, B. W.; McKinnon, J. J.; Spackman, M. A. Polymorphism in 3-methyl-4-methoxy-4′-nitrostilbene (MMONS), a highly active NLO material. *CrystEngComm* **2008**, *10*, 197–206.

[27] Sugiyama, H.; Uekusa, H. Relationship between crystal structures and photochromic properties of *N*-salicylideneaminopyridine derivatives. *CrystEngComm* **2018**, *20*, 2144–2151.

[28] Turner, M. J.; McKinnon, J. J.; Wolff, S. K.; Grimwood, D. J.; Spackman, P. R.; Jayatilaka, D.; Spackman, M. A. *CrystalExplorer 17* **2017**, University of Western Australia. https://crystalexplorer.scb.uwa.edu.au/

[29] Mackenzie, C. F.; Spackman, P. R.; Jayatilaka, D.; Spackman, M. A. CrystalExplorer model energies and energy frameworks: extension to metal coordination compounds, organic salts, solvates and open-shell systems. *IUCrJ* **2017**, *4*, 575–587.

[30] Turner, M. J.; Grabowsky, S.; Jayatilaka, D.; Spackman, M. A. Accurate and efficient model energies for exploring intermolecular interactions in molecular crystals. *J. Phys. Chem. Lett.* **2014**, *5*, 4249–4255.

[31] Grimme, S. Semiempirical GGA-type density functional constructed with a long-range dispersion correction. *J. Comput. Chem.* **2006**, *27*, 1787–1799.

Acknowledgements

This study was financially supported by JSPS Grant-in-Aid for Scientific Research on Innovative Areas “Soft Crystal” (20H04677), the Grant-in-Aid for Research Activity start-up (19K23638), and Waseda University Grant for Special Research Projects (2020C-530). We also would like to thank Prof. Mark Spackman at the University of Western Australia for kindly answering our questions about CrystalExplorer.

Author contributions

D.T. performed all calculations and curated the results. T.A. supervised D.T., and managed lab resources. D.T. and T.T. wrote the paper. T.T. planned and managed this project.

Competing financial interests

The authors declare no competing financial interests.

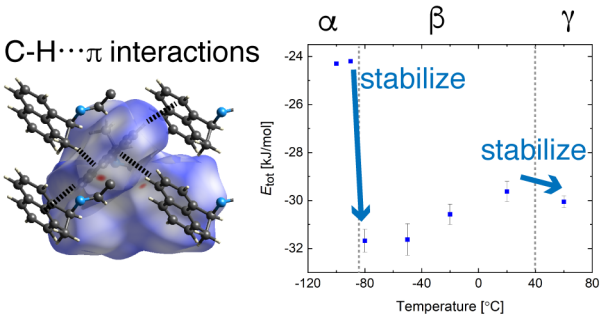

For Table of Contents Only